

and comparative results. The increase in Antarctic sea ice and decrease in Arctic sea ice reported here are consistent with results from a General Circulation Model (GCM) study in which CO₂ levels were increased gradually (4). Other GCM simulations, though, show slight decreases in Antarctic sea ice extent and thickness (3). GCM simulations of CO₂-induced climate change patterns generally agree on some large-scale features such as the amplification of wintertime warming at high northern latitudes but disagree particularly at high southern latitudes (25). This study also indicates a surface air cooling over the Atlantic sector of the Southern Ocean in austral summer (the season when we observe a maximum positive trend in the ice extents). In these GCM experiments, the hemispheric difference in the climate response results in part from the influence of the thermal inertia of the much larger ocean area in the Southern Hemisphere. Sea ice growth in the Southern Ocean, along with slight lowering of the surface water temperature, are attributed to a general freshening of southern circumpolar surface water and the resultant reduction of convective mixing (3, 4). The continuing sea ice data record shows significant interannual and decadal variability that helps provide the basis for developing a better understanding of the various processes driving the observed changes.

REFERENCES AND NOTES

1. R. J. Stouffer, S. Manabe, K. Bryan, *Nature* **342**, 660 (1989).
2. J. M. Murphy and J. F. B. Mitchell, *J. Clim.* **8**, 57 (1995).
3. H. B. Gordon and S. P. O'Farrell, *Mon. Weather Rev.* **125**, 875 (1997).
4. S. Manabe, M. J. Spelman, R. J. Stouffer, *J. Clim.* **5**, 105 (1992).
5. P. Gloersen and W. J. Campbell, *Nature* **352**, 33 (1991).
6. O. M. Johannessen, M. W. Miles, E. Bjørgo, *ibid.* **376**, 126 (1995).
7. E. Bjørgo, O. M. Johannessen, M. W. Miles, *Geophys. Res. Lett.* **24**, 413 (1997).
8. P. Gloersen and F. T. Barath, *IEEE J. Oceanic Eng. OE-2*, 172 (1977).
9. J. P. Hollinger, *DMSP Special Sensor Microwave/Imager Calibration/Validation, Final Report Vol. 1* (Naval Research Laboratory, Washington, DC, 1989).
10. Correction for ice extent and area differences from the various sensors during the overlap periods was critical to obtaining unbiased long-term trends. In Bjørgo *et al.* (7), a correction for SMMR-SSM differences was mentioned but none for SSMI F8-F11 differences. Bjørgo *et al.* used a two-step procedure to match ice concentrations for the SMMR-SSM correction. Our matching of algorithm coefficients was somewhat comparable to their procedure, but then we additionally matched ice extents and areas during the overlap periods.
11. Each data set was subjected to careful quality control, including the identification and subsequent correction or removal of bad data. Residual instrumental drift in the SMMR radiances used in the sea ice algorithm was reduced, by means of a procedure used previously (26), to values well below the instrument noise levels (8). The SSMI drifts similarly determined were found to be below or at the instrument

- noise values (9) for the SSMI radiances used in the sea ice algorithm (19 GHz horizontally and vertically polarized, 22 GHz vertically polarized, and 37 GHz vertically polarized) and so were ignored. Data gaps were filled by performing spatial and temporal interpolations. Additional corrections made to the SMMR and SSMI single-day sea ice concentration grids included the removal of false sea ice signals in the vicinity of the shoreline and over ice-free ocean areas. These were accomplished through the application of a coastline correction algorithm operating on the three image pixels nearest the coast, and also of monthly climatological sea surface temperature thresholds.
12. The calculation of Arctic and Antarctic sea ice concentrations needed to compute sea ice extents and sea ice areas utilizes methods used previously for the SMMR (26) and SSMI (27) data sets. The details of generating a consistent set of sea ice extents and areas from the SMMR and SSMI sensors are discussed elsewhere (28). Since the publication of this report (28), DMSP F13 SSMI data through 31 December 1996 were added, but we followed the same procedure in preparing the data for analysis.
 13. D. J. Cavalieri, K. M. St. Germain, C. T. Swift, *J. Glaciol.* **41**, 455 (1995).
 14. Other differences giving rise to different ice concentrations include differences in sensor altitudes and view angles; differences in weather filter thresholds and algorithm tie points; and different overpass times, tidal phases, and diurnal effects.
 15. The upper limit of the ice extent and area errors for both the Arctic and Antarctic is obtained by calculating the standard deviations of the ice extent and area differences from the F11 and F13 SSMIs during their 5-month overlap period. The estimates are all about 0.3% of the annual mean value. It is noteworthy that the equatorial crossing times of the two spacecraft differ by 45 min, so that even this estimate includes real fluctuations of the ice covers. Of central importance in this study is not absolute accuracy but the consistency of measurements throughout the data record.
 16. C. Kuo, C. R. Lindberg, D. J. Thomson, *Nature* **343**,

- 709 (1990).
 17. C. L. Parkinson and D. J. Cavalieri, *J. Geophys. Res.* **94**, 14499 (1989).
 18. M. C. Serreze, J. A. Maslanik, J. R. Key, R. F. Kokaly, D. A. Robinson, *Geophys. Res. Lett.* **22**, 2183 (1995).
 19. J. E. Walsh, W. L. Chapman, T. L. Shy, *J. Clim.* **9**, 480 (1996).
 20. W. L. Chapman and J. E. Walsh, *Bull. Am. Meteorol. Soc.* **74**, 33 (1993).
 21. G. Kukla and J. Gavin, *Science* **214**, 497 (1981).
 22. H. J. Zwally, C. L. Parkinson, J. C. Comiso, *ibid.* **220**, 1005 (1983).
 23. T. H. Jacka and W. F. Budd, in *International Conference on the Role of the Polar Regions in Global Change*, G. Weller, C. L. Wilson, B. A. B. Severin, Eds. (Geophysical Institute and Center for Global Change and Arctic System Research, University of Alaska, Fairbanks, AK, 1991), pp. 63–70.
 24. C. L. Parkinson, *Antarct. Res. Ser.*, in press.
 25. J. Raisanen, *Clim. Dynam.* **13**, 197 (1997).
 26. P. Gloersen *et al.*, *Arctic and Antarctic Sea Ice, 1978–1987: Satellite Passive Microwave Observations and Analysis* (NASA, SP-511, Washington, DC, 1992).
 27. D. J. Cavalieri *et al.*, *J. Geophys. Res.* **96**, 21989 (1991).
 28. D. J. Cavalieri, C. L. Parkinson, P. Gloersen, H. J. Zwally, *NASA Technical Memorandum 104647* (1997).
 29. The confidence level was determined with a Student's *t* test in which the number of degrees of freedom is obtained by subtracting the number of calculated parameters from the number of windows used in the multiple window filtering.
 30. The SSMI data sets were provided by the National Snow and Ice Data Center in Boulder, CO. We thank S. Fiegles, M. Martino, and J. Saleh for their efforts in reprocessing and correcting the SMMR and SSMI data sets and J. A. Maslanik and J. Stroeve for their help in checking the final sea ice concentrations. This work was supported by NASA's polar program.
- 15 August 1997; accepted 2 October 1997

Abiotic Selenium Redox Transformations in the Presence of Fe(II,III) Oxides

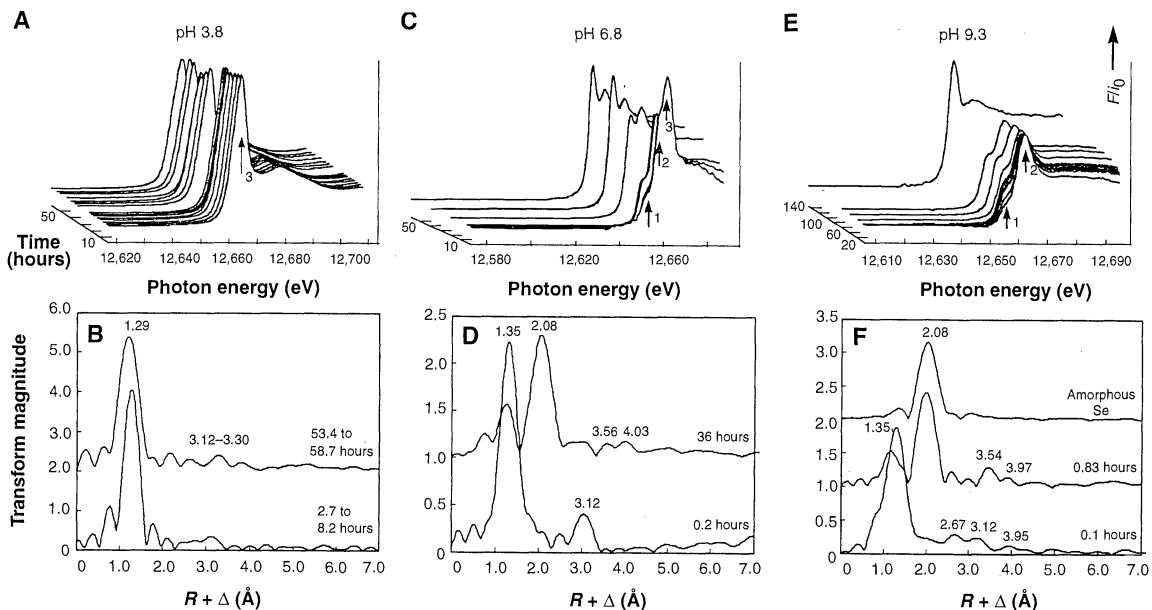
S. C. B. Myneni,* T. K. Tokunaga, G. E. Brown Jr.

Many suboxic sediments and soils contain an Fe(II,III) oxide called green rust. Spectroscopic evidence showed that selenium reduces from an oxidation state of +VI to 0 in the presence of green rust at rates comparable with those found in sediments. Selenium speciation was different in solid and aqueous phases. These redox reactions represent an abiotic pathway for selenium cycling in natural environments, which has previously been considered to be mediated principally by microorganisms. Similar green rust-mediated abiotic redox reactions are likely to be involved in the mobility of several other trace elements and contaminants in the environment.

The redox chemistry of polyvalent elements determines their solubility, bioavailability, and toxicity in geologic environments (1, 2). This is apparent in the case of Se, which occurs in the environment in +VI, +IV, 0, and -II oxidation states and in several organic forms (2–4). Their concentration and biogeochemical transformations determine the activity of Se in the environment. Although Se is essential to animal life at low concentrations and its deficiency is known to cause white muscle

disease in sheep, Se compounds at high concentrations are carcinogenic and teratogenic (4). The higher valent Se forms are more soluble, and their reduction in soil to the less reactive Se(0) form has generally been considered to be facilitated primarily by soil organic acids (5) and microorganisms (6, 7). However, many suboxic geologic environments contain green rust (GR), which is a mixed Fe(II), Fe(III) oxide, and it has been shown to catalyze redox reactions (8–10). Here we show how GR medi-

Fig. 1. Se K-edge XANES (top) and Fourier-transformed EXAFS (bottom) of Se(VI) samples reacted with Fe(II) at different pH (Table 1). At pH 3.8 GR did not precipitate, and the spectra were collected for aqueous species (A and B). (The pH values are ± 0.5 .) Se(VI) coprecipitates with GR in the case of samples (C) to (F), and the spectra correspond to the Se speciation in solid phase (*F* is the Se fluorescence yield and i_0 is the incident beam intensity). The marked peaks 1, 2, and 3 in the XANES spectra represent Se(0), Se(IV), and Se(VI), respectively. Except for (A), the intensities of peaks 2 and 3 decrease and peak 1 increases with time. The

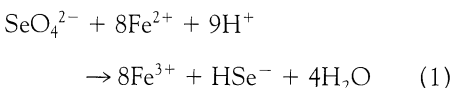


XANES spectra of aqueous phase in contact with GR show Se(VI) only (not shown here). The Fourier transforms of EXAFS spectra shown in (B), (D), and (F) are uncorrected for phase, and the peaks represent complexing atoms around the central x-ray absorber Se. After phase correction, the actual bond lengths are 0.25 to 0.4 Å longer than those shown. (B) Bond length = 1.29 Å, Se-O as in SeO_4^{2-} . Note that Se(VI) reagents contain traces of SeO_3^{2-} (<2%), which exhibits a shoulder at the 1.29 Å Se-O peak (~ 1.35 Å). This also complexes with Fe and produces a weak feature at 3.30

Å corresponding to Se-Fe as in Fe-SeO_3^{2-} . (D) Bond length = 1.35 Å, Se-O in SeO_3^{2-} ; 2.08 Å, Se as in metallic Se; 3.12 Å, two Fe atoms as in bidentate binuclear Fe-SeO_3^{2-} complex; 3.56 Å, distant Fe probably around Se(0); 4.03 Å, distant Fe or Se atoms. (F) Bond length = 2.67 Å, Fe polyhedral edge sharing with SeO_3^{2-} ; and other peaks around 1.35, 2.08, 3.12, 3.54, and 3.97 are the same as those mentioned for (D). *R* and Δ represent the distance and phase shift correction for an absorber and backscatter pair, respectively.

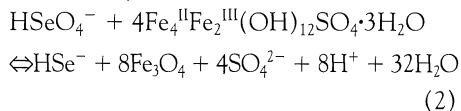
ates abiotic Se reduction.

A survey of standard state redox potentials of Fe and Se species (Fe, species 0, +II, and +III; Se, species -II, 0, +IV, and +VI) suggests that Fe(II) can reduce Se from the +VI oxidation state to the -II form (1, 11, 12). The overall reaction can be written as



Although Fe(II) is present primarily as $\text{Fe}(\text{H}_2\text{O})_6^{2+}$ in acidic solutions, it precipitates as GR, $\text{Fe}(\text{II})_a\text{Fe}(\text{III})_b(\text{OH})_{12}\text{X} \cdot 3\text{H}_2\text{O}$ ($a \rightarrow 4, b \rightarrow 2, \text{X} = \text{interlayer anion}$), in the presence of Fe(III) and at pH > 4.0 and as $\text{Fe}(\text{OH})_2$ in the absence of Fe(III) and pH > 8.0 (13). The common presence of Fe(III) in all iron-containing soils and sediments prevents the formation of $\text{Fe}(\text{OH})_2$ and promotes precipitation of GR. Hence, Se(VI) reduction at pH > 4.0 may occur by homogeneous reactions in aqueous phase and by heteroge-

neous reactions either on GR surfaces by adsorption and reduction or in GR interlayers by coprecipitation and reduction. GR converts to goethite ($\alpha\text{-FeOOH}$), lepidocrocite ($\gamma\text{-FeOOH}$), maghemite ($\gamma\text{-Fe}_2\text{O}_3$), or magnetite (Fe_3O_4), depending on the rate of oxidation and dehydration of GR (13, 14). In our experiments, Se(VI) reduction with GR primarily produced magnetite. On the basis of these mechanisms Se(VI) reduction can be described by the following reaction:



which has a Gibbs free energy change (ΔG°_R) of -671.1 kJ.

We examined these Fe(II)-mediated Se(VI) reduction reactions in closed systems and monitored changes in aqueous- and solid-phase Se speciation as a function of several variables pertinent to natural systems (15). The GR we used had interlayers of SO_4^{2-} , which can coexist with Fe(II) without redox state changes (11, 12). We monitored in situ Se speciation using x-ray absorption near edge structure (XANES) and extended x-ray absorption fine structure (EXAFS) spectroscopy. The precipitate morphology and mineralogy were examined with transmission x-ray microscopy and x-ray dif-

fraction. The energy position of the $1s \rightarrow 4p$ electronic transitions of the Se K-absorption edge shifts to higher energies with an increase in oxidation state and hence is characteristic of the Se oxidation state [the Se +VI, +IV, 0, and -II oxidation states are at 12,665, 12,662, 12,658, and 12,656 eV, respectively] (16). We combined this information with EXAFS data to identify Se local coordination in aqueous and solid phases. Because EXAFS data collection takes several hours for dilute samples, the samples were examined at 10 K to avoid sample modifications. Se(VI) reduction rates at these low temperatures are extremely small. As discussed later, samples with pH less than 4.0 were examined at 298 K because they did not exhibit redox transformations.

In acidic solution (pH $\sim 3.5 \pm 0.5$), where aqueous Fe(II) exists as $\text{Fe}(\text{H}_2\text{O})_6^{2+}$ without any GR precipitate, Se(VI) was not reduced within 160 hours of reaction. The XANES spectra of Se in these samples did not show changes in the energy position of the absorption edge with time (Fig. 1A), which suggests that the Se oxidation state and its local coordination were the same in all samples. EXAFS studies of the same samples did not indicate the presence of Se(VI)-Fe(II) inner- or outer-sphere (ion pair) complexes, and the studies revealed that all added Se(VI) was in the form of uncomplexed

S. C. B. Myneni and T. K. Tokunaga, Earth Sciences Division, Ernest Orlando Lawrence Berkeley National Laboratory, University of California, Berkeley, CA 94720, USA.

G. E. Brown Jr., Department of Geological and Environmental Sciences and Stanford Synchrotron Radiation Laboratory, Stanford University, Stanford, CA 94305, USA.

*To whom correspondence should be addressed.

SeO₄²⁻ (Table 1 and Fig. 1B).

In contrast, aqueous Se(VI) was unstable in the samples prepared at pH > 5.0. Under these conditions GR precipitated initially and, in time, converted to magnetite and lepidocrocite at pH 7.0 and to only magnetite at pH 9.5 (Table 1 and Fig. 2). The presence of GR and its oxidized products in these samples strongly influenced aqueous- and solid-phase Se speciation. When Se(VI) was present during GR precipitation, the aqueous Se concentration dropped quickly [more than 48% in the first 0.01 hour (36 s)] and thereafter decreased slowly with a first-order rate (average rate constant $k = 1.31 \pm 0.63 \times 10^{-2} \text{ hour}^{-1}$) (Table 2). However, the aqueous Se concentration gradually declined at a similar rate (average $k = 1.15 \pm 0.42 \times 10^{-2} \text{ hour}^{-1}$) when Se(VI) interacted with already precipitated

GR. Although Se(VI) can be lost from the aqueous phase by homogeneous reduction to insoluble Se(0) in the presence of high pH Fe(II) species, such as Fe(OH)⁺ and Fe(OH)₂⁰, this reaction was not observed. These solutions were also below saturation for the known Se solids; hence, precipitation is not the mechanism for Se loss (17, 18). These studies demonstrate the necessity of GR for Se(VI) transformations, which may be occurring both in the interlayers and on the external surfaces of GR.

Although aqueous Se speciation did not change at pH > 5.0, all precipitated GR samples exhibited Se(VI) reduction. The degree of reduction varied with pH, the nature of the reaction (coprecipitation versus adsorption), and the initial Fe(II) concentration (15) (Fig. 1, C to F). Se-coprecipitated GR samples reduced Se(VI) rapidly to Se(IV) at high pH when compared with those precipitated around neutral pH (Fig. 1, C and E). Reduced Se(IV) formed bidentate binuclear (at pH 7.0 and 9.3) and edge-sharing complexes (at pH 9.3) with Fe polyhedra, but no Fe-selenite precipitate (Fig. 1, D and F).

This coordination environment changed as the solid-phase Se(IV) was further reduced to Se(0), and GR oxidized simultaneously to magnetite and lepidocrocite. The EXAFS data indicate that the reduced Se(0) atoms occurred as amorphous Se clusters. At reaction times of more than ~60 hours, the Se-absorption edge of the solids shifted to energies lower than that of Se(0), which indicates that trace quantities of Se(-II) were in the system.

In reactions with previously precipitated GR surfaces, Se(VI) reduced directly to Se(0) without detectable accumulation of the Se(IV) intermediate (Fig. 3). Also, Se(0) formed at a slower rate during these adsorption reactions than during the coprecipitation reactions discussed above. Such major changes in the Se speciation of the solid phase may have been a result of incorporation of Se(VI) into the interlayers of GR during coprecipitation and weaker Se(VI) interactions on GR surfaces during adsorption. The interlayer-trapped Se(VI) formed bidentate binuclear and edge-sharing complexes with structural Fe(II) and was reduced immediately to Se(IV), which in turn slowly converted to Se(0) and Se(-II). The invariance in the x-ray diffraction profiles of pure and Se-reacted GR and magnetite and the longer Se(0)-Fe distances of 3.85 Å (from EXAFS, Fig. 1, D and F) suggest that Se(0) substitution inside these mineral structures is unlikely. Se(0) substitution in iron oxides was also not observed from electron microscopy studies (19). On the basis of these results, we hypothesize that the reduction of interlayer-substituted Se(VI) to Se(0) may have promoted magnetite formation at the expense of GR, and the reduced Se(0) atoms formed clusters on surfaces. Although no direct

Table 1. Se(VI) reactions with Fe(II) as a function of pH. The initial concentration of Fe(II) ([Fe(II)]_{initial}) was 7.72 (±0.5) mM and [Se(VI)]_{initial} was 44 (±10) μM in all samples except for A and B in which [Se(VI)]_{initial} was 1.13 mM. The samples A to F were examined by XANES and EXAFS (Fig. 1).

Sample	pH (±0.5)	Remarks
A, B	3.8	Solution, GR absent.
C, D	6.8	GR precipitates initially. Converts to magnetite and lepidocrocite.
E, F	9.3	GR precipitates initially. Converts to magnetite.

Table 2. Rates of Se(VI) loss from aqueous solutions in the presence of Fe(II). Samples 1 and 2 and 3 through 9 represent homogeneous and heterogeneous reactions with GR, respectively. In the case of samples 3 to 6, GR was precipitated in the presence of Se(VI) (coprecipitation); for samples 7 to 9, Se(VI) was added to already precipitated GR. Fe(II) solutions were prepared by dissolving FeSO₄ · 7H₂O, and the reported [Fe(II)]_{initial} represents both Fe(II) and traces of Fe(III) present in the reagent. [Se(VI)]_{initial} was 41 ± 4 μM (Na₂SeO₄). For the estimation of the rate constant for coprecipitation samples (3 to 6), aqueous [Se(VI)]_{initial} was not considered. This is because Se(VI) incorporates into GR structure during its precipitation, and the initial Se(VI) loss from solution has no relation to Se(VI) chemical reduction. N.R., no reaction.

Sample	pH (±0.5)	[Fe(II)] _{initial} (mM)	k (×10 ⁻² hour ⁻¹)
1	4.1	7.78	N.R.
2	4.5	3.22	N.R.
3	10.9	7.73	1.68
4	10.8	3.56	1.04
5	6.3	8.25	1.03
6	6.1	3.66	1.11
7	11.0	7.3	1.42
8	10.6	4.3	1.30
9	6.4	9.54	0.75

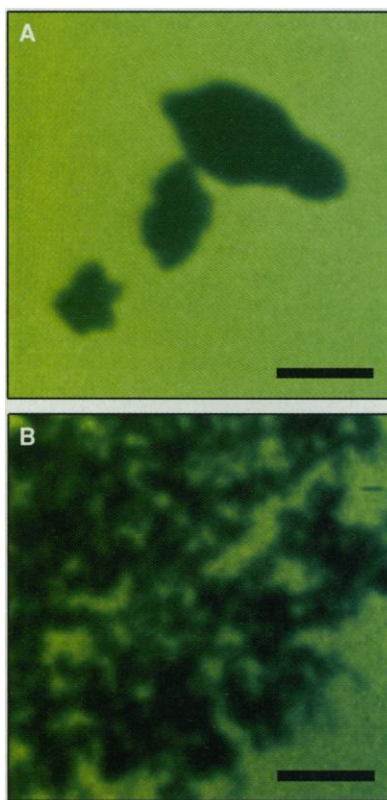


Fig. 2. In situ transmission x-ray microscopy images of Fe(II,III) oxide precipitates (27). (A) GR, prepared by titrating FeSO₄ solution to a pH of ~9.5 with NaOH. (B) Microcrystallites of magnetite and lepidocrocite formed from Se(VI) reactions with GR at pH 7.0. (for Se speciation, refer to Fig. 1D). Scale bar, 0.5 μm. The mineral identification was supported by x-ray diffraction.

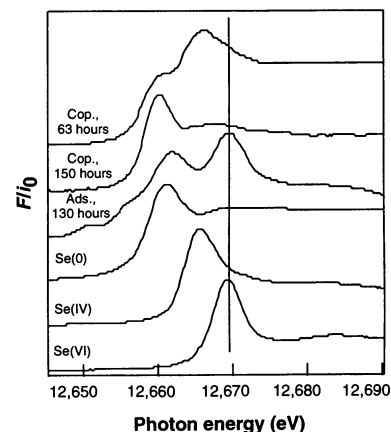


Fig. 3. In situ XANES spectra of a Se(VI) reaction with GR as a function of sorption mechanisms [coprecipitation (Cop.) and adsorption (Ads.)]. The XANES spectra of Se models in different oxidation states are shown for comparison. The vertical line in the center shows the position of Se(VI).

physical evidence was available, similar reaction mechanisms have been proposed for NO_3^- reduction in the presence of GR (9, 10).

We conclude that Se(VI) reduces to Se(IV) and Se(0) in the presence of GR. Although elemental Fe and $\text{Fe}(\text{OH})_2$ are absent in nature, their reactions with Se(VI) in the laboratory produced similar redox transformations (15, 19). Thermodynamically, Se(VI) should reduce to the most stable Se(-II) form in the presence of Fe(II), but we did not observe this species at high concentration. However, it can be a dominant species when the Fe(II) concentration is much higher and the reaction times are longer than those we considered. Se(VI) reduction by coprecipitation and adsorption pathways can occur when anoxic conditions are created in Se-contaminated sediments (16) [reductive dissolution of Fe(III) oxides precipitates GR with Se], as compared with the ion movement into the previously existing anoxic zones containing GR (dominantly adsorption). The Se(VI) transformation rates we measured are within the range of those reported from other laboratory and field studies on Se speciation in sediments and soils (20–23). The pore waters of several natural samples are also saturated with respect to GR, which indicates its probable presence in these systems. The rapid precipitation kinetics (13) and the flexible crystal structure of GR (24) may allow its formation under a variety of geochemical conditions. The reductive dissolution of Fe(III)-oxyhydroxides forms GR steadily in the anoxic sediments; hence, the concentration and final oxidation products of GR are not the limiting factors for the trace element redox reactions. GR-mediated redox reactions similar to those presented here can occur for other trace elements. For instance, studies on Cr(VI) and As(V) reduction have identified the importance of sediment Fe(II)-containing mineral phases as mediators of redox reactions, but attempts to identify these mineral phases are not complete (25, 26). The rapid oxidation of GR poses a problem for its identification during conventional sediment mineralogical analysis, and for this reason this mineral has not been commonly recorded in sediments. However, recent thermodynamic and spectroscopic studies give direct evidence for the existence of GR in soils (8, 13). The abiotic redox reactions we present provide direct evidence for the formation of reduced Se species in anoxic sediments. Although various strains of bacteria have been identified to facilitate Se(VI) reduction in soil and sediment systems, abiotic reactions with GR should be considered when evaluating trace element and major element redox dynamics in sediments and soils.

REFERENCES AND NOTES

- G. Sposito, *The Chemistry of Soils* (Oxford Univ. Press, New York, 1989).
- G. A. Cutter, *Science* **217**, 829 (1982).
- J. H. Howard III, *Geochim. Cosmochim. Acta* **41**, 1665 (1977).
- H. M. Ohlendorf, D. J. Hoffman, M. K. Saiki, T. W. Aldrich, *Sci. Total Environ.* **52**, 49 (1986).
- A. M. Shaker, *J. Colloid Interface Sci.* **180**, 225 (1996).
- R. S. Oremland et al., *Environ. Sci. Technol.* **24**, 1157 (1990).
- C. Garbisu, T. Ishii, T. Leighton, B. B. Buchanan, *Chem. Geol.* **132**, 199 (1996).
- F. Trolard et al., *Geochim. Cosmochim. Acta* **61**, 1107 (1997).
- H. C. B. Hansen, C. B. Koch, H. Nancke-Krog, O. K. Borggaard, J. Sørensen, *Environ. Sci. Technol.* **30**, 2053 (1996).
- C. J. Ottley, W. Davison, W. Edmunds, *Geochim. Cosmochim. Acta* **61**, 1819 (1997).
- K. B. Krauskopf, *Introduction to Geochemistry* (McGraw-Hill, New York, 1979).
- F. M. M. Morel and J. G. Hering, *Principles and Applications of Aquatic Chemistry* (Wiley-Interscience, New York, 1993).
- H. C. B. Hansen, O. K. Borggaard, J. Sørensen, *Geochim. Cosmochim. Acta* **58**, 2599 (1994).
- J. M. Bigham and O. H. Tuovinen, in *Planetary Ecology*, D. E. Caldwell, Ed. (Van Nostrand Reinhold, New York, 1985), pp. 239–250.
- S. C. B. Myneni and G. E. Brown Jr., "Stanford Synchrotron Radiation Laboratory Activity Report" (Stanford University, Stanford, CA, 1997).
- I. J. Pickering, G. E. Brown Jr., T. K. Tokunaga, *Environ. Sci. Technol.* **29**, 2456 (1995).
- M. E. Essington, *Soil Sci. Soc. Am. J.* **52**, 1574 (1988).
- D. Rai, A. R. Felmy, D. A. Moore, *J. Solution Chem.* **24**, 735 (1995).
- R. A. Zingaro, D. C. Dufner, A. P. Murphy, C. D. Moody, *Environ. Int.* **23**, 299 (1997).
- G. R. Jayaweera and J. W. Biggar, *Soil Sci. Soc. Am. J.* **60**, 1056 (1996).
- G. Sposito et al., *ibid.* **55**, 1597 (1991).
- T. K. Tokunaga, I. J. Pickering, G. E. Brown Jr., *ibid.* **60**, 781 (1996).
- P. H. Masscheleyn, R. D. Delaune, W. H. Patrick Jr., *Environ. Sci. Technol.* **24**, 91 (1989).
- I. R. McGill, B. McEnaney, D. C. Smith, *Nature* **259**, 200 (1976).
- L. D. Anderson, D. B. Kent, J. A. Davis, *Environ. Sci. Technol.* **28**, 178 (1994).
- J. M. Brannon and W. H. Patrick Jr., *ibid.*, p. 450.
- The images of mineral grains in 10- μm -thick films of reaction solutions were taken with the high-resolution zone plate microscope, XM-1, which was built and is operated by the Center for X-ray Optics, Lawrence Berkeley National Laboratory (LBNL), Berkeley, CA. See also W. Meyer-Ilse et al., *Synchrotron Radiat. News* **8**, 29 (1995).
- We thank S. M. Benson, J. M. Bigham, G. Sposito, S. J. Traina, G. A. Waychunas, and P. T. Zawislanski for reviewing the manuscript; M. Zavarin and A. Foster for helping with XAS measurements; and W. Meyer-Ilse and J. T. Brown for their collaboration with x-ray microscopy studies. Supported by the Office of Basic Energy Science, Geoscience Program, grant DOE: DE-ACO3-76SF00098 (to T.K.T. and S.C.B.M.); Laboratory Directed Research and Development Fund, LBNL (to S.C.B.M.); and NSF grant EAR-9406490 (to G.E.B.). The Stanford Synchrotron Radiation Laboratory and the Center for X-ray Optics and Advanced Light Source (LBNL) are funded by the U.S. Department of Energy. This is LBNL journal article number LBNL-40832/UC-03.

22 July 1997; accepted 24 September 1997

High-Pressure Transformation of Al_2O_3

Nobumasa Funamori and Raymond Jeanloz

X-ray diffraction measurements indicate that ruby (Cr^{3+} doped $\alpha\text{-Al}_2\text{O}_3$) transforms to the Rh_2O_3 (II) structure when heated to temperatures exceeding ~ 1000 kelvin at pressures above ~ 100 gigapascals, in agreement with predictions from ab initio quantum mechanical calculations. The high-pressure phase did not quench upon decompression to ambient pressure, and the occurrence of this phase transformation may affect interpretations of static (diamond-anvil cell) and dynamic (shock-wave) experiments at ultra-high pressures.

Corundum ($\alpha\text{-Al}_2\text{O}_3$, space group $R\bar{3}c$) is important in many fields of research, for example serving as a model material in ceramic science (1). In high-pressure research, it is used as a window in shock-wave experiments (2), and also as a pressure-transmitting medium for static compression in the diamond-anvil cell (DAC) (3). Moreover, the pressure-induced shift of the Cr^{3+} fluorescence wavelength of ruby (Cr^{3+} doped $\alpha\text{-Al}_2\text{O}_3$) is used as a pressure calibrant in DAC experiments (4). Theoretical calculations on the behavior of corundum at high pressures (5–7) predict that $\alpha\text{-Al}_2\text{O}_3$ will transform to the Rh_2O_3 (II)

structure (space group $Pbcn$) (8). Recent calculations, based either on pseudopotential (7) or on linearized augmented plane-wave (6) methods, yield a transition pressure of 78 to 91 GPa, raising the possibility that the ruby-fluorescence pressure scale may be contaminated by the effects of a structural transformation. However, no evidence of a transformation was observed in a high-pressure x-ray diffraction study on ruby to 175 GPa (9), and it has therefore been assumed that the $\alpha\text{-Al}_2\text{O}_3$ structure is stable to this pressure.

To clarify whether there is a transformation, we carried out a high-pressure in situ x-ray diffraction experiment on ruby that had been heated to a temperature exceeding ~ 1000 K while at high pressure (10).

Department of Geology and Geophysics, University of California, Berkeley, CA 94720-4767, USA.